### Title

A new URCA process




### Journal

The Astrophysical Journal, 424(1)

### ISSN

0004-637X



### Authors

Aufderheide, Maurice B
Fushiki, Ikko
Fuller, George M
et al.



### Publication Date

1994-03-01

### DOI

10.1086/173887

Peer reviewed

THE ASTROPHYSICAL JOURNAL, 424:257–262, 1994 March 20


# A NEW URCA PROCESS

MAURICE B. AUFDERHEIDE,[1] IKKO FUSHIKI,[2] GEORGE M. FULLER,[3] AND THOMAS A. WEAVER[4]

*Received 1993 February 2; accepted 1993 September 23*

## ABSTRACT

In the course of a general study of electron capture and $\beta$-decay rates on fp shell nuclei which are abundant after core silicon burning in massive stars, we have found that the Fuller, Fowler, and Newman $\beta$-decay rates are much stronger than generally has been realized. In fact, they can balance the capture rates during the conditions which are prevalent after core silicon burning, resulting in a new Urca process. The strength of the $\beta$-decay rates is a result of thermal population of the Gamow-Teller back resonance in the parent nucleus and the behavior of $\beta$-decay and electron capture $Q$-values for ensembles of nuclei in nuclear statistical equilibrium. All $\beta$-decay rate tabulations prior to Fuller, Fowler, and Newman neglected the contribution of back resonances and thus drastically underestimated the overall rate. We use a simple analytic model to explain this balancing. The full rates are coupled to a nuclear statistical equilibrium code to demonstrate the strength of the decays. One zone models are used to examine, in a self-consistent fashion, how these rates could affect the presupernova evolution of the iron core and hence the core collapse problem.

*Subject headings:* nuclear reactions, nucleosynthesis, abundances — stars: interiors — supernovae: general

## 1. INTRODUCTION

The importance of Gamow-Teller (G-T) resonances in enhancing stellar electron capture rates in the fp shell was first proposed by Bethe et al. (1979). Fuller, Fowler, & Newman (FFN) (1980, 1982a, 1982b, 1985) were the first to systematically include these resonances in calculations of stellar electron capture rates for 226 nuclei with $A$ less than or equal to 60. Weaver, Woosley, & Fuller (1985) showed that, in massive stars before core collapse, the effect of these new rates was to cause a greater reduction in the electron fraction, $Y_e$, because of captures to the G-T resonance region, FFN also calculated $\beta^{\pm}$ decay rates, but the FFN $\beta^-$ decay rates have never been used in the KEPLER (Weaver, Zimmerman, & Woosley 1978) stellar evolution code. There are two reasons for this omission. Earlier calculations of stellar $\beta$-decay rates (Hansen 1966, 1968; Mazurek 1973; Mazurek, Truran, & Cameron 1974) had indicated that these decay rates were much weaker than the capture rates with resonances included. Also, the difficulty of adequately fitting the FFN $\beta$-decay rates discouraged such an effort.

In this paper we would like to call attention to the actual character of the FFN $\beta$-decay rates. These rates are much stronger than the previous rates calculated by Hansen (1966, 1968) and Mazurek et al. (1974). In § 2 we show analytically why the $\beta$-decays can balance the electron capture rates. The source of this enhancement in rate is the same as it is for capture rates: the G-T resonance in the electron capture direction. We also discuss the $Q$-value effects which enhance the decay phase space. In § 3 the full FFN rates are coupled to a nuclear statistical equilibrium (NSE) code and the $\rho$, $T$, and $Y_e$ trajectories of the center of 15 $M_\odot$ and 25 $M_\odot$ stellar models are followed. The strength of the decays and their prodigious neutrino emission are shown. In § 4 the effect of the decays on these trajectories is studied self-consistently, using one-zone models. A true Urca process (Gamow & Schoenberg 1941) is seen, resulting in a cooler, less neutron-rich zone. In § 5 the relevance of this new physics for Type II supernova collapse is discussed.

## 2. WHY THE RATES BALANCE

Figure 1 illustrates the distribution of G-T strength for a generic fp shell nucleus. The resonant strength in the electron capture direction is typically 1 MeV to 10 MeV above the daughter ground state. This strength is 10 to 100 times larger than the low-lying transitions measured in fp shell nuclei. At the conditions just after silicon core burning (temperature $\sim 3.3 \times 10^9$ K, density $\sim 10^8$ g cm$^{-3}$, and $Y_e \sim 0.47$), the electron chemical potential, $\mu_e$ is on the order of 2 MeV, so that a significant fraction of the electrons are able to capture from the parent state to the G-T resonance, significantly enhancing the rate.

For $\beta$-decay, the giant G-T resonance is not typically in the decay phase space. Thus, the problem appears to require calculating matrix elements for weak transitions between many low-lying states. However, because the nuclei are thermally excited, this situation is avoided, at least in this stage of stellar evolution. Consider constructing the $\beta$-decay rate for the nucleus (Z–1, A) shown in Figure 1. If the temperature is high enough, the resonance obtained by starting at (Z, A) and going to (Z–1, A) will be thermally populated. These states, called the "back resonance", will decay to the ground state of (Z, A) with a very large matrix element (which can be obtained by detailed balance from the inverse reaction). Because of the size of these matrix elements, they quickly dominate the $\beta$-decay rate. The decay rates become so large that they can balance the $e^-$ capture rates.

Let us compare the electron capture rate of (Z, A) and the $\beta$-decay rate of (Z–1, A). Let the nuclear mass difference between (Z–1, A) and (Z, A) be $Q_0(>0)$. Let the G-T resonance be $E_{\rm GTR}$ above the ground state of (Z–1, A), and let its matrix element by $|M|^2$. We assume that the electron capture rate is

[1] E Division and IGPP, L-413, Lawrence Livermore National Laboratory. Postal address: Physics Department, University of Pennsylvania, Philadelphia, PA 19104-6396.
[2] Ink Development Corporation, 1300 South El Camino Real, Suite 201, San Mateo, CA 94402.
[3] Physics Department, University of California, San Diego, La Jolla, CA 92093-0319.
[4] General Studies Group, Physics Department, Lawrence Livermore National Laboratory, Livermore, CA 94550.

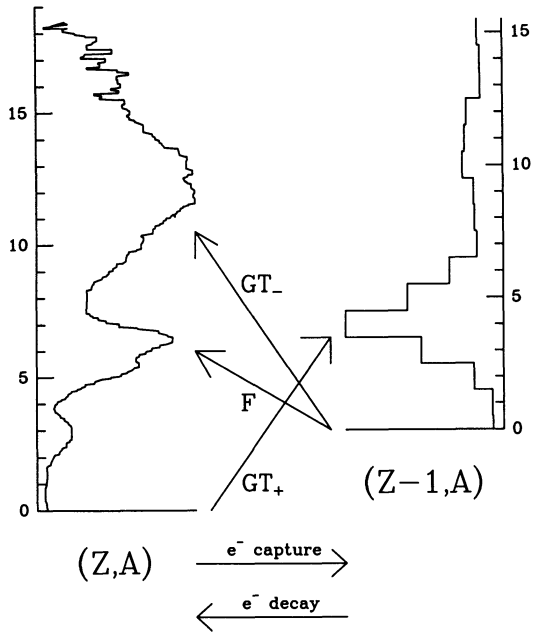


FIG. 1.—General distribution of G-T strength in fp shell nuclei. Operating on the ground state of nucleus (Z, A) with the G-T$_+$ operator produces the allowed G-T strength function displayed in the (Z–1, A) nucleus. This is the electron capture direction and is probed by intermediate energy ($n$, $p$) reactions. Similarly, operating on the ground state of nucleus (Z–1, A) with the G-T$_-$ operator produces the allowed G-T strength function displayed in the (Z, A) nucleus. This is the $\beta$-decay direction and is probed by intermediate energy ($p$, $n$) reactions. Note that it is possible to thermally populate the resonant states in the parent nucleus which decay strongly to the daughter ground state. These strength functions exist for each parent and daughter excited state and must all be included when calculating the stellar rates.

dominated by captures to the G-T resonance and that the $\beta$-decay rate is dominated by thermal population of the G-T resonance. These assumptions are generally valid when either rate is important. If nuclear spins and partition functions are neglected for clarity, the decay rate can then be approximated by

$$\lambda^{\rm bd}_{Z-1,A} \approx |M|^2 \exp\left[\frac{-E_{\rm GTR}}{k_B T}\right] \times \left[\int_0^{\mu} dp p^2 (q-p)^2 \exp\left(\frac{p-\mu}{\tau}\right) + \int_{\mu}^{q} dp p^2 (q-p)^2\right], \quad (1)$$

where $q$, $\mu$, and $\tau$ are $Q_0 + E_{\rm GTR}$, $\mu_e$, and $k_B T$, respectively, all scaled by $m_e c^2$. The electron capture rate can be approximated by

$$\lambda^{\rm ec}_{Z,A} \approx |M|^2 \int_q^{\infty} dp p^2 (q-p)^2 \exp\left(\frac{\mu - p}{\tau}\right). \quad (2)$$

We have assumed that $Q_0 > \mu_e \gg m_e$, fairly accurate when these rates are important, and have used the methods described in § V of FFN (1982a).

The conditions which are relevant for the presupernova environment are $T \approx 0.3$ MeV and $\mu_e \approx 2$ MeV. FFN typically place their resonances several MeV above the ground state, so let $E_{\rm GTR} = 3$ MeV. Under these conditions, $\lambda^{\rm bd}_{Z-1,A}/\lambda^{\rm ec}_{Z,A}$ is a rapidly increasing function of $Q_0$. For these conditions, equality is reached at $Q_0 = 2.2$ MeV. As the material becomes more neutron rich, the average $Q_0$ increases. Thus the presupernova environment naturally encounters conditions under which decays can compete with electron captures.

This point is illustrated in a heuristic way in Figure 2. As the star evolves, the gas becomes more and more neutron rich. The NSE ensemble thus begins to move toward the right (the neutron-rich) side of the figure. As this happens, the mass differences between the nuclei become larger and larger. Thus, for a given nucleus, electron captures from it must surmount an ever-increasing barrier, while $\beta$-decays from the nucleus involve increasing drops to more bound nuclei. Although the $\beta$-decay phase-space integral is inherently weaker than the electron capture integral, this difference in $Q$-values is what allows the balancing shown above to occur. It should be noted that this trend does not continue into core collapse because of the electron chemical potential. As the evolution proceeds, density increases, leading to larger values of $\mu_e$. By densities of $5 \times 10^9$ g cm$^{-3}$, the electron gas is so degenerate that the $\beta$-decays are completely blocked.

It should also be noted that the arguments made here for the balancing of electron capture and $\beta$-decay are only true if the resonances are treated consistently. If the back resonance is left out of the $\beta$-decay rate, the balancing will never be seen. In such a case, the electron captures through the G-T resonance will dominate the relatively weak $\beta$-decays completely. This is one reason why the balancing described here has never been seen before. Previous work has used FFN electron capture rates and older decay rates without the back resonance.

## 3. THE RATES ON STELLAR TRAJECTORIES

As part of a search for nuclei beyond $A = 60$ which could contribute to the evolution of $Y_e$ in presupernova evolution, we (Aufderheide et al. 1993) have coupled a computer code which calculates abundances of nuclei in NSE to the FFN rates. The NSE code uses experimentally measured atomic masses where known (Wapstra & Audi 1985) and the mass law of Comay, Kelson, & Zidon (1988) for all other nuclei. For the results in

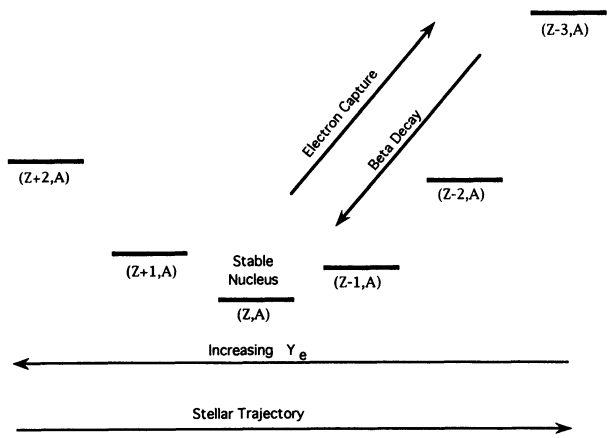


FIG. 2.—Trend in $Q$-values along a stellar trajectory. The masses of several nuclei with atomic mass $A$ are plotted. Typically, there is one stable nucleus, surrounded by nuclei of greater mass. As one moves away from the stable, most bound nucleus, the mass differences become larger and larger. $\beta$-decay reactions proceed from right to left in this figure, while electron captures proceed from left to right. As the stellar trajectory becomes more neutron rich, the $\beta$-decays became more favorable, since they can proceed "downhill," while electron captures must proceed "uphill." As evolution proceeds, this difference becomes large enough that the $\beta$-decays are able to balance the electron captures, as shown in § 2.

this paper, the mass of most of the nuclei is known, and so the choice of mass law is not particularly relevant.

The rate of change in $Y_e$, due to the $k$th nucleus, is given by

$$\dot{Y}_e^{\mathrm{ec(bd)}}(k) = -(+)\frac{X}{A}\lambda_k^{\mathrm{ec(bd)}}, \quad (3)$$

where $X$ is the mass fraction of the $k$th nucleus (Z, A) and $\lambda_k^{\mathrm{ec(bd)}}$ is the electron capture ($\beta$-decay) rate for this nucleus. The coupling of abundances with the FFN rates allow us to compare the relative contributions of the FFN $e^-$ capture and decay rates to $\dot{Y}_e$ for conditions relevant to presupernova evolution. This is the first time such a study has been done on the full FFN rates. $\dot{E}^{\mathrm{ec(bd)}}$, the rate of energy release in neutrinos due to $e^-$ capture ($\beta$-decay), is also computed. Including nuclei with $A > 60$ does not alter the conclusions of this paper.

In Figures 3*a–d* we plot $\dot{Y}_e$ and $\dot{E}$ for the center of a 15 $M_\odot$ star (the s15s7b2 stellar model) and a 25 $M_\odot$ star (the s25s7b8 stellar model) as core silicon burning is ending. These stars were evolved using the KEPLER stellar evolution code (Weaver et al. 1978) with the FFN $e^-$ capture rates (Weaver et al. 1985) and some $\beta$-decay rates from Hansen (1966, 1968), Mazurek (1973) and Mazurek et al. (1974). We have used the values of density, temperature, and $Y_e$ for these trajectories as inputs for our calculation of $\dot{Y}_e$ and $\dot{E}$. Stars with mass between roughly 12 $M_\odot$ and 30 $M_\odot$ exhibit a bifurcation in behavior at roughly 20 $M_\odot$; stars below this mass have cooler, higher density cores, while stars above this mass have hotter, lower density cores. The two models we have chosen are exemplars of each case. We are thus probing the general conditions for stellar evolution after core silicon burning for any star with mass between roughly 12 $M_\odot$ and 30 $M_\odot$. The curves in Figure 3 truly reflect what is happening in the star only after $Y_e$ is below roughly 0.47. Before this, the material has not completed core silicon burning and is not in NSE. Note that in the 25 $M_\odot$ model, the higher temperatures and lower densities result in the energy emitted by neutrino-antineutrino pairs, $\dot{E}^{\nu\bar{\nu}}$, being much stronger than in the 15 $M_\odot$ case.

As Figures 3*a* and 3*c* show, just after core silicon burning is complete, the $e^-$ capture reactions dominate. But as $Y_e$ drops, neutron-rich nuclei with large beta decay rates become abundant. At $Y_e \approx 0.456$ in both stars, the capture and decay rates balance. Following these trajectories further is no longer consistent because the calculations from which it was derived did not use these large decay rates. This example shows that the decays could be important in the evolution. It can be seen in Figures 3*b* and 3*d* that after balancing of $Y_e$ has occurred, the energy emission from $\beta$-decay neutrinos becomes very large—100 times larger than any other emission process. This indicates that the decays might significantly cool the core before collapse, but nothing definite can be said without including the decays in the calculation.

The effects seen in Figure 3 are fairly robust. They are not the result of a single nucleus decaying. Many nuclei have rapid decay rates because the G-T back resonance is a general

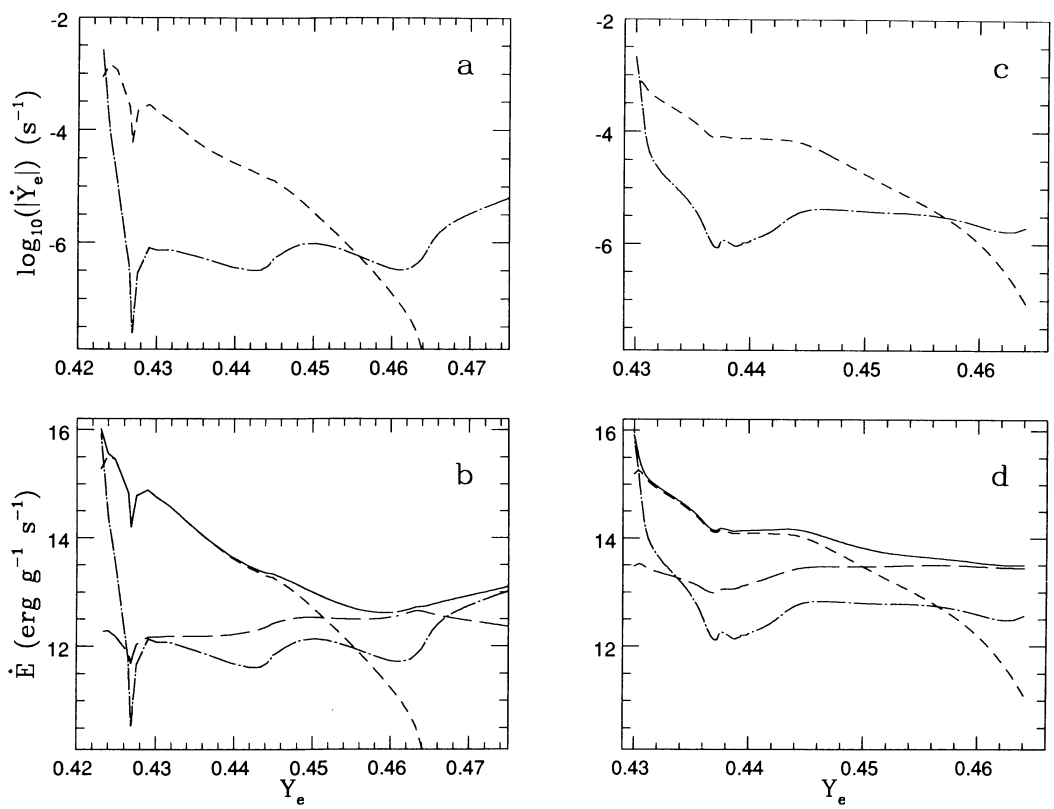


FIG. 3.—Evolution of $\dot{Y}_e$ (*a* and *c*) and $\dot{E}$ (*b* and *d*) along the stellar trajectory. The 15 $M_\odot$ case is on the left, while the 25 $M_\odot$ case is on the right. The evolution begins on the right of each plot and proceeds to ever lower values of $Y_e$. In (*a*) and (*c*) the dash-dot line is $\dot{Y}_e^{\mathrm{ec}}$, and the dashed line is $\dot{Y}_e^{\mathrm{bd}}$. In (*b*) and (*d*) the dash-dot line is $\dot{E}^{\mathrm{ec}}$, the short-dashed line is $\dot{E}^{\mathrm{bd}}$, the long-dashed line is $\dot{E}^{\nu\bar{\nu}}$, and the solid line is the total $\dot{E}$. The nearly discontinuous nature of the curves for $Y_e \approx 0.427$ (15 $M_\odot$) and 0.438 (25 $M_\odot$) is the result of silicon shell burning episodes which temporarily relieve the core pressure. Note that just before the end of the evolution, electron captures again dominate because of the increasing density.

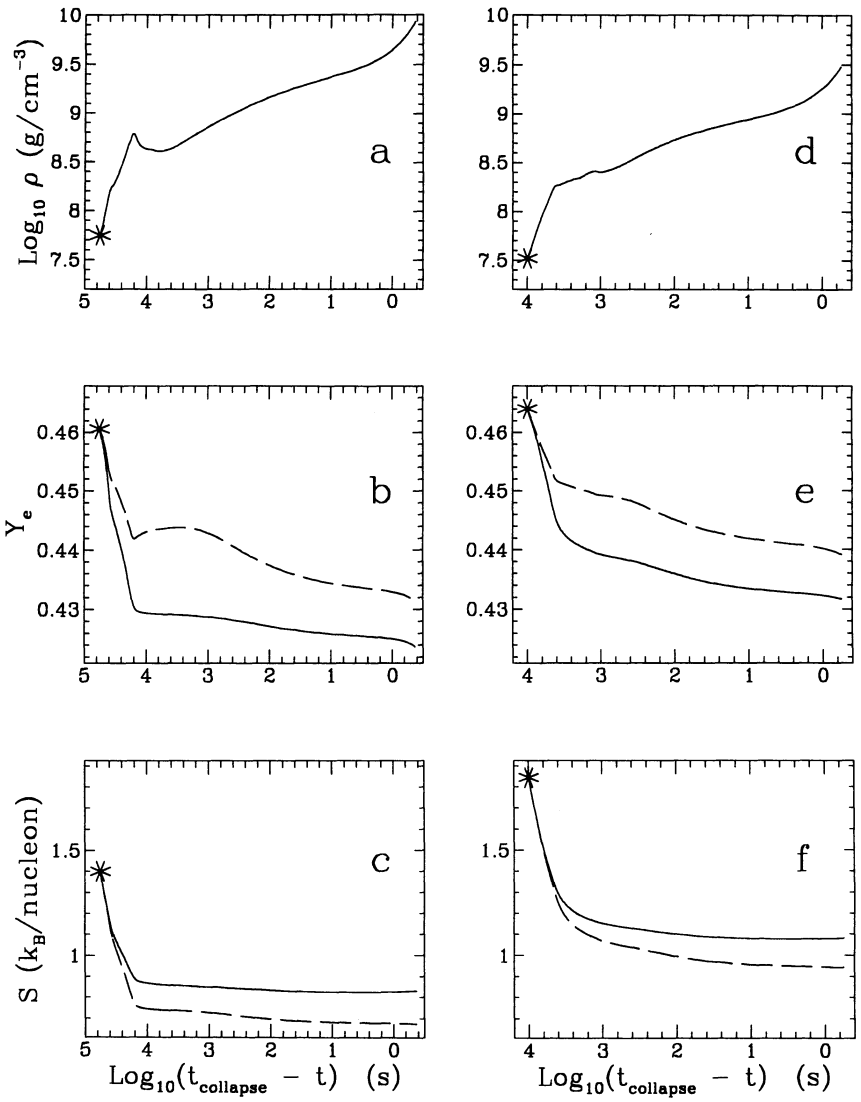


FIG. 4.—Evolution of (*a*) and (*d*) $\rho$, (*b*) and (*e*) $Y_e$, and (*c*) and (*f*) $S$ with time. The $15\,M_\odot$ model is on the left and the $25\,M_\odot$ model is on the right. The solid line is the original $15\,M_\odot$ trajectory, which does not use the FFN beta decay rates. The dashed line is our one zone calculation, which uses all of the FFN electron capture and $\beta$-decay rates. The asterisk in each plot shows where the one-zone model started. The reductions in density approximately $10^{4.2}$ s and $10^3$ s before collapse in the $15\,M_\odot$ and $25\,M_\odot$ cases, respectively, are results of the silicon shell burning episodes mentioned in Fig. 3. The minor reduction in density approximately $10^{4.6}$ s before collapse in the $15\,M_\odot$ model is the result of an oxygen shell burning phase.

feature of all unblocked fp shell nuclei (Fuller 1982). Thus, this behavior is different from what was discussed by Aufderheide et al. (1990). They had suggested that several $A > 60$ nuclei with large $\beta$-decay $Q$-values could cool the core. Such a scenario is prevented for two reasons. First, as has been seen here, the decays are dominated by back resonances and not by which nucleus has a large $Q$-value. Second, the nuclei mentioned by Aufderheide et al. (1990) are not very abundant in the core until just before collapse. The effects seen in this paper have a larger effect because they occur much earlier in the evolution and many nuclei contribute.

## 4. ONE-ZONE MODELS

The effect of the decays can be investigated in a self-consistent fashion with a one-zone approach similar to that of Fuller (1982). In this technique, $\rho(t)$ for a point in the star is taken from a full calculation, and the new physical processes are added to the calculation. It is assumed that the processes added to the calculation will not significantly alter the hydrodynamic evolution. Using initial conditions from the original model, one steps forward by $\delta t$. Let the subscript 0 refer to all quantities at time $t$ and subscript 1 refer to all quantities at time $t + \delta t$. The quantity $\rho_1$ is determined from the given profile. $Y_{e,1}$ is calculated from

$$Y_{e,1} = Y_{e,0} + \dot{Y}_{e,0}\,\delta t\,. \tag{4}$$

All that remains is to determine $T_1$, and then we have fully advanced to $t + \delta t$. This is done by using the first law of thermodynamics,

$$dE + P\,dV = dQ = T\,dS + \sum_i \mu_i\,dY_i\,, \tag{5}$$

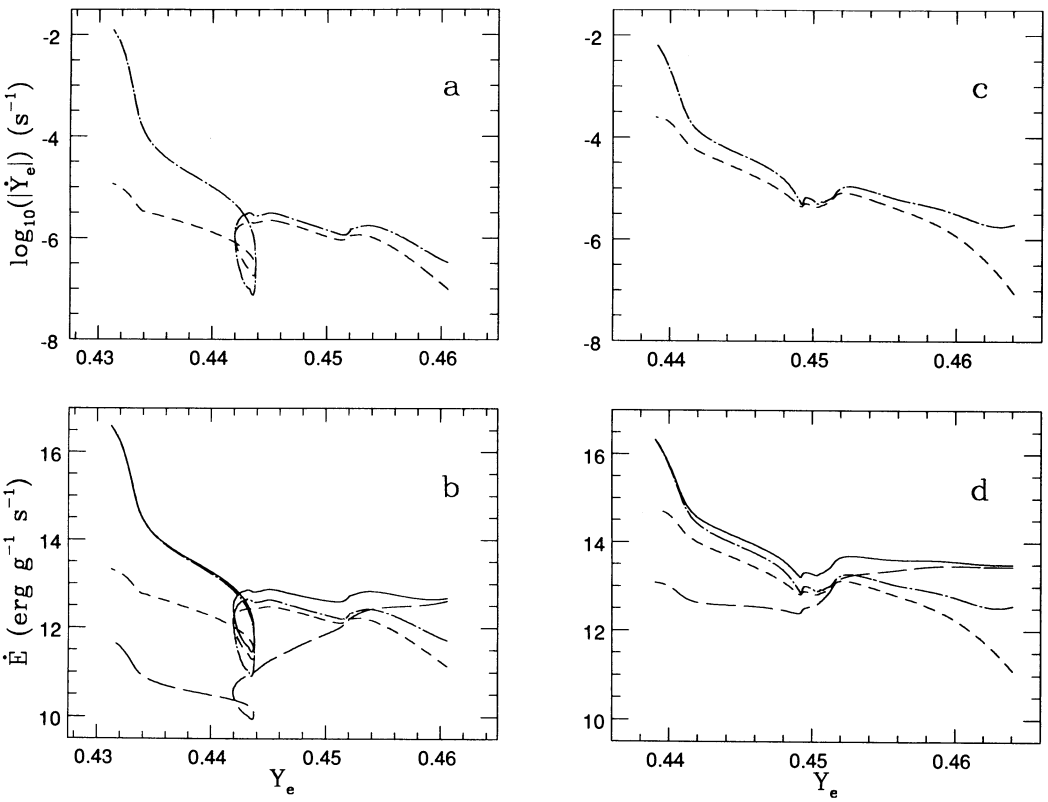


FIG. 5.—(*a*) and (*c*) Evolution of $\dot{Y}_e$ and (*b*) and (*d*) $\dot{E}$ along the one-zone trajectories. The 15 $M_\odot$ case is on the left, while the 25 $M_\odot$ case is on the right. The evolution begins on the right of each plot and proceeds to ever lower values of $Y_e$. In (*a*) and (*c*), the dash-dot line is $\dot{Y}_e^{ec}$, and the dashed line is $\dot{Y}_e^{bd}$. In (*b*) and (*d*), the dash-dot line is $\dot{E}^{ec}$, the short-dashed line is $\dot{E}^{bd}$, the long-dashed line is $\dot{E}^{\nu,\bar{\nu}}$, and the solid line is the total $\dot{E}$.

where $Y_i = X_i/A_i$, $X_i$ is the mass fraction of species $i$, $\mu_i$ is the chemical potential of the $i$th species, and all quantities are per nucleon. Note that $\mu_e dY_e$ is one of the terms in the sum over species. The heat flow through the zone, $dQ$, is determined in this case by the neutrino emission processes, and so equation (5) can be rewritten as

$$dS = \frac{(-\dot{E}^{ec} - \dot{E}^{bd} - \dot{E}^{\nu,\bar{\nu}})\delta t - \sum_i \mu_i dY_i}{T}, \qquad (6)$$

where $\dot{E}^{\nu,\bar{\nu}}$ is the energy emission from neutrino-antineutrino pair production processes. This change in entropy allows us to compute the new entropy, $S_1 = S_0 + dS$. We iterate this equation until we obtain a temperature, $T_1$, which satisfies it. The new trajectory for $Y_e$ and $T$ is then calculated by repeating this process and following $\rho(t)$.

In Figures 4*a–f*, we compare the $Y_e(t)$ and $S(t)$ profiles obtained from the evolution of the 15 $M_\odot$ and 25 $M_\odot$ models with our one-zone calculation in which we have included the FFN $\beta$-decay rates. It can be seen that the $\beta$-decays have a large effect on the subsequent evolution of $Y_e$ and entropy. $Y_e$ decreases more slowly in the one-zone model because of the $\beta$-decays, which increase $Y_e$. In both models, $Y_e$ is 0.008 units larger at collapse. Because the new trajectory is less neutron rich than the original one, the beta decay $\dot{Y}_e$ and $\dot{E}$ are not as large as in Figure 3. The balancing of rates which we saw at $Y_e \approx 0.456$ in Figure 3 does not actually occur until $Y_e \approx 0.442$ in the 15 $M_\odot$ model and $Y_e \approx 0.45$ in the 25 $M_\odot$ model. The entropy exhibits impressive changes from the original trajectory. At the end of the calculations, the entropy of the material is 0.15 Boltzmann units less, corresponding to a drop in temperature to $T_9 = 6.76$ (7.63) from the original value of $T_9 = 8.48$ (8.40) in the 15 (25) $M_\odot$ model. The enhanced efficiency of the $\beta$-decay cooling is evident.

Although the capture and decay rates balance near $Y_e \approx 0.446$, $\beta$ equilibrium has not been reached because the neutrinos are not yet trapped; rather, a dynamic equilibrium, a true Urca process, is occurring. An interesting feature of this Urca process is that it is actually a sum of many individual Urca cycles. No single cycle is balanced, but the net effect is a robust balance. In this respect, this Urca process is quite different from the original Urca process of Gamow & Schoenberg (1941).

In Figures 5*a–5d*, we have plotted $\dot{Y}_e$ and $\dot{E}$ along the one-zone trajectories for the 15 $M_\odot$ and the 25 $M_\odot$ models, for comparison with Figure 3. It can be seen that the feedbacks from the $\beta$-decays, both from cooling and from following a less neutron-rich trajectory, prevent the decay rates from overwhelming the captures. In the 15 $M_\odot$ case, it can be seen that a more vigorous Urca process has occurred. In fact, $Y_e$ has actually increased for a short while (the source of the loops in Figs. 5*a* and 5*b*).

These changes in $Y_e$ and $T_9$ have opposing effects on the pressure in the gas. As a result, for the 15 (25) $M_\odot$ model, there is only a 0.45% (1%) decrease in the total pressure (relative to the cases without $\beta$-decays) of the material $10^4$ ($10^3$) s before collapse. It is not clear how such small changes in pressure will affect the hydrodynamics of the evolution, but at least the one-zone models have not affected the pressure by a large

amount. Full stellar evolution calculations using all of the FFN rates will be necessary to determine the full effects of the $\beta$-decay rates. This one-zone calculation does show that the $\beta$-decays are important in forming the initial models for core collapse.

## 5. CONCLUSIONS

The decay rates must be put into stellar evolution calculations as soon as possible. An effort is underway to include these rates in KEPLER. It is likely that their effect will be to produce iron cores with a central $Y_e$ of 0.43–0.44 and lower entropies than are seen in the present cores. It is also clear that any calculation of $\beta$-decay rates for massive star evolution must include the back resonance if they are to be relevant for the conditions seen after core silicon burning.

The FFN rates have been available for almost 10 yr and one might wonder why this Urca process has only been discovered now. The main reason is that no one had ever constructed the tools necessary to see the effect. As was discussed in § 2, this balancing is as much an effect of the NSE ensemble as it is of the FFN rates. Without a knowledge of the abundances of the nuclear gas, it is not possible to put the FFN rates in the proper astrophysical context. Stellar evolution codes do couple this information, but none had included the FFN $\beta$-decay rates. Bethe et al. (1979) saw the importance of the G-T resonance for electron capture, but not for $\beta$-decay. As a result, when the FFN tables became available, the electron capture rates were included in stellar evolution codes as quickly as possible, and compared against older decay rates. Since the old decay rates did not include back resonances, it appeared that electron capture was the dominant weak reaction in the presupernova regime. Because of the amount of work required to include the decays in stellar evolution codes, and their apparent lack of importance, the inclusion of FFN decays in stellar evolution codes had been deferred while other problems were investigated.

We conclude with a brief discussion of why this result is relevant for core collapse calculations. The one-zone models discussed above indicate that the iron core will have $Y_e$ and entropy profiles which are altered near the center. At the center, $Y_e$ will be larger by roughly 0.01 units, and the entropy will be smaller by roughly 0.15 $k_B$ nucleon$^{-1}$. Somewhere in the inner part of the iron core, these new profiles will smoothly join to the present profiles, in the part of the core where the $\beta$-decays have not yet "turned on." During the collapse, the slightly larger $Y_e$ may allow the shock wave to form slightly further out in the core (Burrows & Lattimer 1983; Cooperstein, Bethe, & Brown 1984), but such a small change could be washed out by the complex feedbacks in the system.

The change in entropy is more interesting. A change of 0.15 $k_B$ nucleon$^{-1}$ is a large effect. During collapse, the formation of the shock wave is very sensitive to the entropy (Bruenn 1989; Baron & Cooperstein 1990), because the entropy determines the number of free protons evaporated from the nuclei. These free protons are the main source of neutronization during collapse, thus helping to set where the shock wave forms in the core. A lower central entropy, as seen here, would lead to a smaller number of free protons, less neutronization, and hence a shock formed further out in the core. Models 104, 109, and 110 of Baron & Cooperstein (1990) demonstrate these features. The reductions in entropy which they examined were less strong than what has been seen here and they saw major enhancements in the resulting shock waves. It is thus clear that these $\beta$-decays could have an effect on the nature of the collapse and subsequent explosion of Type II supernovae.

M. B. A. thanks N. A. Gentile, F. D. Swesty, G. E. Brown, M. Prakash, and J. Lattimer for useful discussions of this work. Work at LLNL was performed under the auspices of the US Department of Energy under contract W-7405-ENG-48, DOE nuclear theory grant SF-ENG-48, and DOE contract number DOE-AC02-76-ERO-3071. We also acknowledge support from grants NSF PHY-9121623 and IGPP92-08.

## REFERENCES

Aufderheide, M. B., Brown, G. E., Kuo, T. T. S., Stout, D. B., & Vogel, P. 1990, ApJ, 362, 241
Aufderheide, M. B., Fushiki, I., Woosley, S. E., & Hartmann, D. H. 1993, ApJS, in press
Baron, E., & Cooperstein, J. 1990, ApJ, 353, 597
Bethe, H. A., Brown, G. E., Applegate, J., & Lattimer, J. M. 1979, Nucl. Phys. A, 324, 487
Bruenn, S. 1989, ApJ, 340, 995
Burrows, A., & Lattimer, J. 1983, ApJ, 270, 735
Comay, E., Kelson, I., & Zidon, A. 1988, Atomic Data Nucl. Data Tables, 39, 235
Cooperstein, J., Bethe, H. A., & Brown, G. E. 1984, Nucl. Phys. A, 429, 527
Fuller, G. M. 1982, ApJ, 252, 741
Fuller, G. M., Fowler, W. A., & Newman, M. J. 1980, ApJS, 42, 447
———. 1982a, ApJ, 252, 715
Fuller, G. M., Fowler, W. A., & Newman, M. J. 1982b, ApJS, 48, 279
———. 1985, ApJ, 293, 1
Gamow, G., & Schoenberg, M. 1941, Phys. Rev., 59, 539
Hansen, C. J. 1966, Ph.D. thesis, Yale Univ.
———. 1968, Ap&SS, 1, 499
Mazurek, T. J. 1973, Ph.D. thesis, Yeshiva Univ.
Mazurek, T. J., Truran, J. W., & Cameron, A. G. W. 1974, Ap&SS, 27, 261
Wapstra, A. H., & Audi, G. 1985, Nucl. Phys. A, 432, 1
Weaver, T. A., Woosley, S. E., & Fuller, G. M. 1985, in Numerical Astrophysics: In Honor of J. R. Wilson, ed. J. Centrella, J. LeBlanc, & R. Bowers (Portola: Science Book Internat.), 374
Weaver, T. A., Zimmerman, G. B., & Woosley, S. E. 1978, ApJ, 225, 1021
Woosley, S. E., Pinto, P. A., & Weaver, T. A. 1988, Proc. Astron. Soc. Australia, 7, 355